

Trotter errors in digital adiabatic quantum simulation of quantum \mathbb{Z}_2 lattice gauge theory

Xiaopeng Cui¹ and Yu Shi^{1,*}

¹*Department of Physics & State Key Laboratory of Surface Physics,
Fudan University, Shanghai 200433, China*

Abstract

Trotter decomposition is the basis of the digital quantum simulation. Asymmetric and symmetric decompositions are used in our GPU demonstration of the digital adiabatic quantum simulations of 2 + 1 dimensional quantum \mathbb{Z}_2 lattice gauge theory. The actual errors in Trotter decompositions are investigated as functions of the coupling parameter and the number of Trotter substeps in each step of the variation of coupling parameter. The relative error of energy is shown to be closely related to the Trotter error usually defined in terms of the evolution operators. They are much smaller than the order-of-magnitude estimation. The error in the symmetric decomposition is much smaller than that in the asymmetric decomposition. The features of the Trotter errors obtained here are useful in the experimental implementation of digital quantum simulation and its numerical demonstration.

International Journal of Modern Physics B (2020) 2050292.

<https://doi.org/10.1142/S0217979220502926>

* yushi@fudan.edu.cn

I. INTRODUCTION

Lattice gauge theory (LGT) is the approach to gauge theories based on discretizing the spacetime or space to a lattice. The simplest LGT is \mathbb{Z}_2 LGT, which was first presented as a quantum spin model [1–3]. It is important in particle physics [4–6], condensed matter physics [2, 3, 7–9], as well as quantum computing [10–12]. With the progress of quantum computing, quantum simulation of quantum \mathbb{Z}_2 LGT becomes a possibility [13–17], including analog and digital approaches. Analog quantum simulation is based on mapping the theory to a similar Hamiltonian of a simulating system. Digital quantum simulation is based on Trotter decompositions of the evolution operator [14], including asymmetric decomposition [17–19] and symmetric decomposition [17, 20, 21], among others. The computational complexity, expressed in terms of the number of steps in the Trotter decomposition, depends directly on the Trotter error.

Recently, a digital quantum simulation of quantum \mathbb{Z}_2 LGT is designed using quantum adiabatic algorithm implemented in terms of universal quantum gates, and a classical demonstration of this scheme was made thoroughly in a GPU simulator [17]. Dubbed pseudoquantum simulation, classical demonstration of quantum simulation in state-of-art fast computers facilitates the development of quantum algorithms and quantum softwares, and is also a new approach of computation [17].

In real quantum computing experiments, in order to complete the quantum process before decoherence, it is crucial to reduce the number of Trotter steps as far as the error is acceptable. So it is important to precisely investigate the errors.

In this paper, we perform the pseudoquantum simulation of quantum \mathbb{Z}_2 LGT, and study how the errors depend on the step numbers of decompositions. The accurate Trotter errors numerically obtained turn out to be much smaller than the previous order-of-magnitude estimation. This provides useful information for experimental implementation of the quantum simulation and the parameter selection in pseudoquantum simulation.

II. ORDER-OF-MAGNITUDE ESTIMATION OF THE TROTTER ERRORS OF ADIABATIC QUANTUM SIMULATION OF QUANTUM \mathbb{Z}_2 LGT

A. quantum \mathbb{Z}_2 LGT

Consider the Hamiltonian of the quantum \mathbb{Z}_2 LGT defined on a square lattice [1, 3],

$$H = Z + gX, \quad (1)$$

with

$$X = - \sum_l \sigma_l^x, \quad (2)$$

$$Z = \sum_{\square} Z_{\square}, \quad (3)$$

$$Z_{\square} = - \prod_{l \in \square} \sigma_l^z, \quad (4)$$

where g is the coupling parameter, l represents links on the square lattice, \square represents a plaquette, the smallest loop formed by links. On a square lattice, a plaquette is a square.

The adiabatic evolution starts with the ground state $|\psi_0\rangle$ for $g = 0$, in which $Z_{\square} = -1$ for each plaquette \square [17]. In our original algorithm, g is increased from 0 adiabatically as $g_{k,m} = (k-1)g_s + m\delta$, ($m = 1, \dots, n$), n is the total number of substeps for each step k , g_s is the increase of g in each step, which lasts time t_s , $\delta = g_s/n$ is the increase of g in each substep m . This generalizes the Trotter asymmetric and symmetric decompositions to the case that the Hamiltonian varies at each step m of the Trotter decomposition, which is renamed a substep. The errors in these decompositions were estimated.

Here we simplify the matter and consider g vary only at the end of each step, while remain unchanged in the n Trotter substeps within each step, that is,

$$g_{k,m} = g_k = (k-1)g_s, \quad (5)$$

which remains constant for $m = 1, \dots, n-1$, and increases only when $m = n$. This is because we shall study the dependence of the error on n . If g varies at each decomposition step m , the degree of adiabaticity increases with n , reducing the error due to nonadiabaticity [22]. To focus on the error due to Trotter decomposition, we now fix the rate of g variation, as given in (5).

B. Definitions and estimation of Trotter errors

For the asymmetric Trotter decomposition, the error in each step of g variation consisting of n Trotter substeps is

$$\varepsilon_s^{asy}(t_s, n, g) \equiv \langle \psi(g) | \left((e^{-iZ \frac{t_s}{n}} e^{-igX \frac{t_s}{n}})^n - e^{-iHt_s} \right) | \psi(g) \rangle. \quad (6)$$

For the symmetric Trotter decomposition, the error in each step of g variation consisting of n Trotter substeps is

$$\varepsilon_s^{sym}(t_s, n, g) \equiv \langle \psi(g) | \left((e^{-iZ \frac{t_s}{2n}} e^{-igX \frac{t_s}{n}} e^{-iZ \frac{t_s}{2n}})^n - e^{-iHt_s} \right) | \psi(g) \rangle. \quad (7)$$

One can estimate the Trotter errors under the assumption that t_s/n is very small [17].

By using the identity $e^{A+B} = e^A e^B e^{-\frac{1}{2}[A,B] + \dots}$, we obtain

$$\varepsilon_s^{asy}(t_s, n, g) \approx O\left[\frac{1}{2}gN_p n_l \frac{t_s^2}{n}\right], \quad (8)$$

where N_p is the number of plaquettes, n_l is the number of links in each plaquette. In the derivation, it has been considered that each Z_\square is noncommutative with $n_l \sigma^x$'s. O represents the order of magnitude.

For the symmetric Trotter decomposition, by using the identity $\ln(e^{A/2} e^B e^{A/2}) = A + B - ([A, [A, B]] + 2[B, [A, B]])/24 + \dots$, we obtain

$$\varepsilon_s^{sym}(t_s, n, g) \approx O\left[\left(\frac{1}{12}g^2 N_p n_l^2 + \frac{1}{24}g N_l n_p^2\right) \frac{t_s^3}{n^2}\right], \quad (9)$$

where N_l is the number of links, n_p is the number of plaquettes sharing each link. In the derivation, it has been considered that each Z_\square is noncommutative with $n_l \sigma^x$'s, hence $[Z_\square, X]$ is the sum of n_l products of one σ^y and $n_l - 1 \sigma^z$'s. Each σ^y is noncommutative with the n_p Z_\square 's of the plaquettes sharing with the link l . On the other hand, each product of one σ^y and $n_l - 1 \sigma^z$'s is noncommutative with $n_l \sigma^x$'s. Therefore $[Z, [Z, X]] = O(N_p n_l n_p) = O(N_l n_p^2)$, as $N_p = N_l n_p / n_l$, while $[X, [Z, X]] = O(N_p n_l^2)$. Another way of reasoning is the following. Each σ^x is shared by n_p plaquettes, thus $[Z, \sigma_l^x]$ yields n_p products of one σ^y and $n_l - 1 \sigma^z$'s. Each product is noncommutative with Z_\square 's of the n_p plaquettes, and with the $n_l \sigma^x$'s on the same plaquette. Consequently, $[Z, [Z, X]] = O[N_l n_p^2]$, $[X, [Z, X]] = O[N_l n_p n_l]$. With $N_p = N_l n_p / n_l$, this is the same as above.

Therefore the accumulated total errors are

$$\varepsilon^{asy}(g) = \sum_{k=1}^{N_s(g)} \varepsilon_s^{asy}(t_s, n, kg_s) = \sum_{k=1}^{g/g_s} O\left(\frac{1}{2}kg_s N_p n_l \frac{t_s^2}{n}\right) = O\left(\frac{g(g+g_s)}{4g_s} N_p n_l \frac{t_s^2}{n}\right) \quad (10)$$

for the asymmetric decomposition, and

$$\begin{aligned} \varepsilon^{sym}(g) &= \sum_{k=1}^{N_s(g)} \varepsilon_s^{sym}(t_s, n, kg_s) = \sum_{k=1}^{g/g_s} O\left(\left[\frac{1}{12}(kg_s)^2 N_p n_l^2 + \frac{1}{24}kg_s N_l n_p^2\right] \frac{t_s^3}{n^2}\right) \\ &= O\left[\frac{g(g+g_s)(2g_s n_l^2 N_p + 4g n_l^2 N_p + 3N_l n_p^2)}{144g_s} \frac{t_s^3}{n^2}\right] \end{aligned} \quad (11)$$

for the symmetric decomposition.

In this paper, we consider two-dimensional 3×3 square lattice with periodic boundary condition, for which $N_p = 9$, $N_l = 18$, $n_p = 2$, $n_l = 4$, as shown in Fig. 1. Therefore

$$\varepsilon^{asy}(g) = O\left[\frac{9g(g+g_s)}{g_s} \frac{t_s^2}{n}\right], \quad (12)$$

$$\varepsilon^{sym}(g) = O\left[\frac{g(g+g_s)(288g_s + 576g + 216)}{144g_s} \frac{t_s^3}{n^2}\right] \quad (13)$$

Fig. 2 shows the estimation of the errors as functions of g and n . In our adiabatic simulation, g varies from 0 to 2 adiabatically in steps of $g_s = 0.001$ and time $t_s = 0.1$. It can be seen that the symmetric Trotter has lower error than the asymmetric Trotter. As t is proportional to g in the adiabatic process, $t = (g/g_s)t_s$, the dependence of the error on t is just the dependence on $(t_s/g_s)g$.

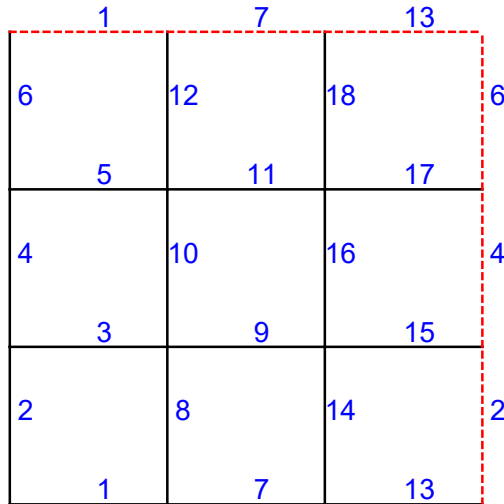


FIG. 1. Two-dimensional 3×3 lattice, with periodic boundary condition. The links are numbered.

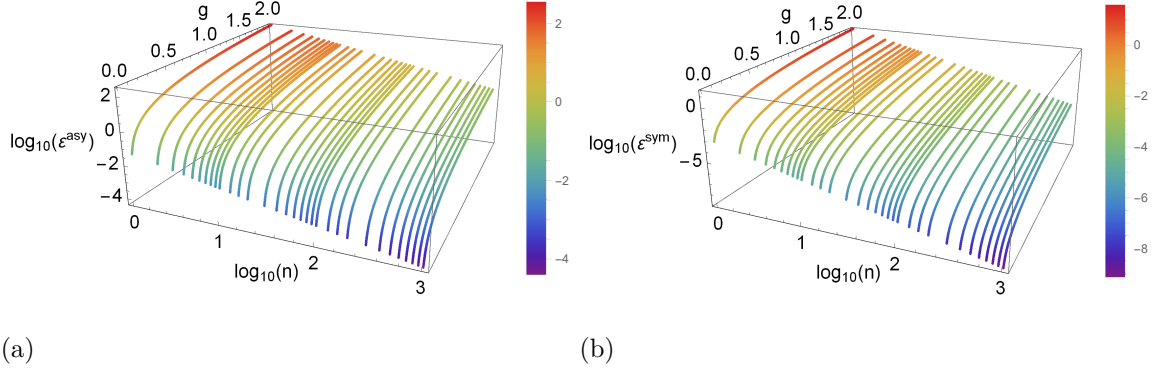


FIG. 2. Order-of-magnitude estimated Trotter errors as functions of g , which increases from 0 to 2 in steps of $g_s = 0.001$ and $t_s = 0.1$, and $\log_{10} n$, which increases from 0 to 3. (a) Accumulated error ε^{asy} for asymmetric Trotter decomposition. (b) Accumulated error ε^{sym} for symmetric Trotter decomposition.

The above order-of-magnitude estimation is for very small values of t_s/n . Moreover, it is based on assuming that the order of magnitude of the expectation value of each Pauli matrix is 1. So in a sense it is an upper bound. Below we calculate the actual error, which could be much lower.

III. ENERGY ERRORS AND ACTUAL TROTTER ERRORS

The number of Trotter steps n determines the time complexity of the adiabatic quantum simulation. Hence it is crucial to know the actual errors. In the following, we describe our method to evaluate the actual errors.

Let's consider the key physical quantity, namely the energy, and define the expectation value

$$E_0(g) \equiv \langle \psi(g) | H(g) | \psi(g) \rangle = \mathcal{Z}_0(g) + g\mathcal{X}_0(g), \quad (14)$$

with

$$\mathcal{Z}_0(g) \equiv \langle \psi(g) | Z | \psi(g) \rangle \quad (15)$$

$$\mathcal{X}_0(g) \equiv \langle \psi(g) | X | \psi(g) \rangle, \quad (16)$$

which are exact, without Trotter errors. Similarly we also consider the expectation values at the state which are calculated using the Trotter decomposition,

$$E_n(g) \equiv \langle H(g) \rangle_n = \mathcal{Z}_n(g) + \mathcal{X}_n(g), \quad (17)$$

with

$$\mathcal{Z}_n(g) \equiv \langle Z \rangle_n, \quad (18)$$

$$\mathcal{X}_n(g) \equiv \langle X \rangle_n, \quad (19)$$

where the subscript n means that the number of steps in the Trotter decomposition is n . The difference $E_n(g) - E_0(g)$ is a measure of the error in the Trotter decomposition.

Now we connect energy error with the Trotter errors $\varepsilon_s^{asym}(t_s, n, g)$ and $\varepsilon_s^{sym}(t_s, n, g)$ defined in (6) and (7), respectively.

Suppose starting from a same state $|\psi(g)\rangle$, after one step of varying g consisting of n Trotter substep, the exact state is $e^{-iHt_s}|\psi(g)\rangle$, the state computed by an approximating operator F is $F|\psi(g)\rangle$. $F = (e^{-iZ\frac{t_s}{n}}e^{-igX\frac{t_s}{n}})^n$ for the asymmetric Trotter decomposition, and $F = (e^{-iZ\frac{t_s}{2n}}e^{-igX\frac{t_s}{n}}e^{-iZ\frac{t_s}{2n}})^n$ for the symmetric Trotter decomposition.

Then $E_n(g) - E_0(g) \approx \langle \psi(g) | F^\dagger H F | \psi(g) \rangle - \langle \psi(g) | e^{-iHt_s} H e^{-iHt_s} | \psi(g) \rangle$, where we have approximated $|\psi(g - s_s)\rangle$ as $|\psi(g)\rangle$, because of adiabaticity $g_s \ll g$. We define the operator

$$R = F - e^{-iHt_s}. \quad (20)$$

The expectation value of R ,

$$\varepsilon_s \equiv \langle \psi(g) | R | \psi(g) \rangle,$$

is nothing but the Trotter error as defined in (6) and (7). There, the order-of-magnitude estimation is also made.

R is small, hence $F^\dagger H F = (e^{iHt_s} + R^\dagger)H(e^{-iHt_s} + R) \approx e^{iHt_s} H e^{-iHt_s} + e^{iHt_s} H R + R^\dagger H e^{-iHt_s}$, where the higher order term $R^\dagger R$ is neglected. Therefore, $E_n(g) - E_0(g) \approx \langle \psi(g) | (e^{iHt_s} H R + R^\dagger H e^{-iHt_s}) | \psi(g) \rangle$. Using the fact that $H|\psi(g)\rangle = E_0(g)|\psi(g)\rangle$, we have $\langle \psi(g) | (e^{iE_0(g)t_s} R + e^{-iE_0(g)t_s} R^\dagger) | \psi(g) \rangle = (E_n(g) - E_0(g)) / E_0(g)$. We can define

$$\begin{aligned} r(g) &\equiv \langle \psi(g) | (e^{iE_0(g)t_s} R + e^{-iE_0(g)t_s} R^\dagger) | \psi(g) \rangle \\ &= 2\text{Re}(\varepsilon_s e^{iE_0(g)t_s}) \\ &= 2|\varepsilon_s| \cos(E_0(g)t_s + \arg \varepsilon_s), \end{aligned}$$

thus

$$r(g) = \frac{E_n(g) - E_0(g)}{E_0(g)}. \quad (21)$$

Therefore we have shown that the Trotter error ε_s , as defined in (6) or (7) is simply related to the relative error of the energy.

Thought not directly related to Trotter errors in (6) or (7), the relative errors of Z and X can also be defined similarly as

$$\frac{\mathcal{Z}_n(g) - \mathcal{Z}_0(g)}{\mathcal{Z}_0(g)}, \frac{\mathcal{X}_n(g) - \mathcal{X}_0(g)}{\mathcal{X}_0(g)}.$$

There are no exact solutions of $\mathcal{Z}_0(g)$, $\mathcal{X}_0(g)$ and $E_0(g)$. Nevertheless, we can obtain very good approximations by using symmetric Trotter decomposition with very large number of Trotter steps, say, $n = 10^4$, and with the same values of $g_s = 0.001$ and $t_s = 0.1$ as for $E_n(g)$. This benchmark has the additional advantage that there is some cancellation of the nonadiabatic errors, even though they are small, which exist as the variation of g is not infinitesimally slow. $E_0(g)$, $\mathcal{Z}_0(g)$ and $\mathcal{X}_0(g)$ obtained in this way are shown in Fig. 3.

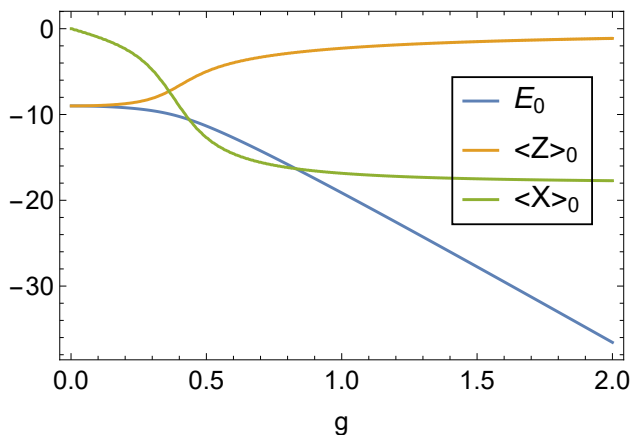


FIG. 3. Good approximations of the expectation values E_0 , $\mathcal{Z}_0 \equiv \langle Z \rangle_0$ and $\mathcal{X}_0 \equiv \langle X \rangle_0$ of H , Z and X , respectively, without Trotter error, as functions of g , obtained by using the symmetric Trotter decomposition with steps of $g_s = 0.001$, $t_s = 0.1$ and $n = 10^4$.

IV. NUMERICAL RESULTS IN THE PSEUDOQUANTUM SIMULATION

We perform pseudoquantum simulation using the QuEST GPU quantum simulator with double precision [23], and using Tesla V100 card of Nvidia GPU. In our pseudoquantum simulation, for each set of values of n and g , we calculate the expectation values We vary n from 1 to 1000, and numerically calculate the characteristic quantities.

A. Energy Errors

$E_n(g) - E_0(g)$ is shown in Fig. 4, where it can be seen that it is two orders of magnitude lower in the symmetric decomposition than in the asymmetric decomposition.

Fig. 4 also shows $\mathcal{Z}_n(g) - \mathcal{Z}_0(g)$ and $\mathcal{X}_n(g) - \mathcal{X}_0(g)$, which are of the same order of magnitude. Moreover, $\mathcal{Z}_n(g) - \mathcal{Z}_0(g)$ in both decompositions are nearly the same. $\mathcal{Z}_n(g) - \mathcal{Z}_0(g)$ is positive. In asymmetric decomposition, $\mathcal{X}_n(g) - \mathcal{X}_0(g)$ is also positive, hence $E_n(g) - E_0(g)$ is the sum of two positive numbers. In symmetric decomposition, $\mathcal{X}_n(g) - \mathcal{X}_0(g)$ is negative, hence $E_n(g) - E_0(g)$ is a sum of one positive number and one negative number. Consequently, $E_n(g) - E_0(g)$ is significantly smaller in the symmetric decomposition than in asymmetric decomposition.

B. Error bounds

There are oscillations in the errors. So we define the error bound of the energy as

$$\varepsilon_H(g) = \max\{|E_n(g') - E_0(g')|\}, \quad (22)$$

where the maximum is over

$$g - \frac{\Delta g}{2} \leq g' \leq g + \frac{\Delta g}{2},$$

with Δg representing a certain window length. After some trials, we find $\Delta g = 0.04$ is about a small suitable value to get rid of the oscillations. The error bounds $\varepsilon_H(g)$ calculated from $E_n(g) - E_0(g)$ in Fig. 4 are shown in Fig. 5. We have also calculated $\varepsilon_H(g)$ for more values of n , which are shown as functions of g in log-normal plots in Fig. 6, as functions of n in log-log plots in Fig. 7, and as functions of n and g in three-dimensional plots in Fig. 8.

Similarly, the error bounds for Z and X are defined as

$$\varepsilon_Z(g) = \max\{|\mathcal{Z}_n(g') - \mathcal{Z}_0(g')|\}, \quad (23)$$

and

$$\varepsilon_X(g) = \max\{|\mathcal{X}_n(g') - \mathcal{X}_0(g')|\}, \quad (24)$$

with the window length for each case also found to be 0.04. ε_Z and ε_X as functions of g and n are shown in Fig. 9.

For quantum \mathbb{Z}_2 LGT, there is a QPT at $g_c \approx 0.38$. It can be seen from Fig. 5, Fig. 6 and Fig. 8 that for the asymmetric decomposition, the dependence of ε_H on g exhibits a significant change when g is increased from $g < g_c$ to $g > g_c$, from an exponential to a linear function. For the symmetric decomposition, there is no such significant change, and ε_H remains a polynomial function of g .

It also can be seen from Fig. 4 and Fig. 9 that in asymmetric and symmetric decompositions, ε_Z 's are the same, for the reason given above about $\mathcal{Z}_n(g) - \mathcal{Z}_0(g)$, but ε_X 's are quite different. For symmetric decomposition, ε_Z and ε_X are close to each other at each value of n and g , because $\mathcal{Z}_n(g) - \mathcal{Z}_0(g)$ and $\mathcal{X}_n(g) - \mathcal{X}_0(g)$ are close in magnitude but opposite in sign, hence their cancellation reduces ε_H .

In either decomposition, ε_Z remains very small when $g < g_c$, and increases linearly with g when $g > g_c$. When $g < g_c$, ε_X increases exponentially with g in asymmetric decomposition, while remains as small as ε_Z in symmetric decomposition. When $g > g_c$, in asymmetric decomposition, ε_X tends to be nearly unchanged, and thus the error bound of gX increases linearly with g , while in symmetric decomposition, ε_X remains close to ε_Z . These behaviors of errors and error bounds of Z and X can explain that of H . Especially, within the parameter regime investigated here, ε_H in symmetric decomposition is two orders of magnitude lower than that in asymmetric decomposition.

Fig. 7, Fig. 8 and Fig. 9 also indicate that in either decomposition, ε_H , ε_Z and ε_X are almost inversely proportional to n , in consistent with the order-of-magnitude estimation of the errors.

C. Relative errors

We now turn to the relative errors.

$r(g) \equiv (E_n(g) - E_0(g))/E_0(g)$ is shown in Fig. 10, where it can be seen that it is also two orders of magnitude lower in the symmetric decomposition than in the asymmetric decomposition. In the asymmetric decomposition, for $g > g_c$, the relative error $r(g)$ is nearly independent of g .

Fig. 10 also shows $(\mathcal{Z}_n(g) - \mathcal{Z}_0(g))/\mathcal{Z}_0(g)$ and $(\mathcal{X}_n(g) - \mathcal{X}_0(g))/\mathcal{X}_0(g)$, with the latter about one order of magnitude less. As $\mathcal{X}_0(g)$ is extremely small when g is very small, $(\mathcal{X}_n(g) - \mathcal{X}_0(g))/\mathcal{X}_0(g)$ is calculated for $g > 0.06$. $(\mathcal{Z}_n(g) - \mathcal{Z}_0(g))/\mathcal{Z}_0(g)$ in both decompo-

sitions are nearly same. While $(\mathcal{Z}_n(g) - \mathcal{Z}_0(g)) / \mathcal{Z}_0(g)$ is positive $(\mathcal{Z}_n(g) - \mathcal{Z}_0(g)) / \mathcal{Z}_0(g)$ is negative, as $\mathcal{Z}_0(g)$ is negative. Similarly, in asymmetric decomposition, $(\mathcal{X}_n(g) - \mathcal{X}_0(g)) / \mathcal{X}_0(g)$ is also negative, hence $(E_n(g) - E_0(g)) / E_0(g)$ is the sum of two negative numbers. In symmetric decomposition, $(\mathcal{X}_n(g) - \mathcal{X}_0(g)) / \mathcal{X}_0(g)$ is positive, hence $(E_n(g) - E_0(g)) / E_0(g)$ is a sum of one negative number and one positive number. Consequently, $(E_n(g) - E_0(g)) / E_0(g)$ is significantly smaller in the symmetric decomposition than in asymmetric decomposition.

D. Relative Error bounds

We define the relative error bound of the energy as

$$\varepsilon_H^r(g) = \max\left\{\frac{|E_n(g') - E_0(g')|}{|E_0(g')|}\right\}, \quad (25)$$

where the maximum is over

$$g - \frac{\Delta g}{2} \leq g' \leq g + \frac{\Delta g}{2},$$

with Δg representing a certain window length, which is also $\Delta g = 0.04$. The error bounds $\varepsilon_H^r(g)$ calculated from $(E_n(g) - E_0(g)) / E_0(g)$ in Fig. 10 are shown in Fig. 11. We have also calculated $\varepsilon_H^r(g)$ for more values of n , which are shown as functions of g in log-normal plots in Fig. 12, as functions of n in log-log plots in Fig. 13, and as functions of n and g in three-dimensional plots in Fig. 14.

Similarly, the relative error bounds for Z and X are defined as

$$\varepsilon_Z^r(g) = \max\left\{\frac{|\mathcal{Z}_n(g') - \mathcal{Z}_0(g')|}{|\mathcal{Z}_0(g')|}\right\}, \quad (26)$$

and

$$\varepsilon_X^r(g) = \max\left\{\frac{|\mathcal{X}_n(g') - \mathcal{X}_0(g')|}{|\mathcal{X}_0(g')|}\right\}, \quad (27)$$

with the window length for each case also being 0.04. ε_Z^r and ε_X^r as functions of g and n are shown in Fig. 9.

It can also be seen from Fig. 11, Fig. 12 and Fig. 14 that for the asymmetric decomposition, the dependence of ε_H^r on g exhibits a significant change when g is increased from $g < g_c$ to $g > g_c$, namely, from an exponential increase to independence of g . For the symmetric decomposition, there is no such a significant change.

It also can be seen from Fig. 10 and Fig. 15 that in asymmetric and symmetric decompositions, ε_Z^r 's are the same, but ε_X^r 's are quite different.

Fig. 7, Fig. 8 and Fig. 9 also indicate that in either decomposition, ε_H^r , ε_Z^r and ε_X^r are almost inversely proportional to n . This feature is shared by order-of-magnitude estimation of the Trotter errors.

V. SUMMARY

Trotter decomposition is the basis of digital quantum simulation. Here we have investigated the errors of symmetric and asymmetric Trotter decompositions and make comparisons between them, and with the order-of-magnitude estimation. Using a GPU simulator, we have performed the numerical demonstration of digital adiabatic quantum simulation of quantum \mathbb{Z}_2 LGT, an approach called pseudoquantum simulation.

We have defined the errors in the energy, and in expectation values of Z and X , the two competing terms in the Hamiltonian. Each error is defined as the difference with the exact expectation value without the Trotter error, which is well approximated by using the Trotter decomposition with a very large number of steps. We have also defined the error bounds to get ride of small oscillations.

For symmetric and asymmetric Trotter decomposition, and for various numbers of substeps, we calculate the errors as functions of the coupling parameter g .

We observed clearly the characteristic differences between asymmetric and symmetric Trotter decompositions. In the symmetric decomposition, the errors in $\langle Z \rangle$ and $\langle X \rangle$ are close in magnitude but opposite in sign, hence the error and error bound in energy are about two orders of magnitude lower than in the asymmetric decomposition.

In the asymmetric and symmetric decomposition, errors and thus the error bounds of $\langle Z \rangle$ are the same, but those of $\langle X \rangle$ are different.

In the asymmetric decomposition, the error bound ε_H increases exponentially with g for $g < g_c$, and increases linearly with g for $g > g_c$. In the symmetric decomposition, ε_H always increases with g polynomially.

We have also investigated the relative errors and their bounds. Especially, we found that the relative error of energy is equal to the Trotter error defined in terms of the evolution operator. The relative error bound of energy can be compared with the order-of-magnitude estimation for the Trotter errors, indicating that the actual error is much lower than the order-of-magnitude estimation, especially when n is very small.

In each decomposition, each actual error is in inverse proportion to n . This relation is the same as in the order-of-magnitude estimation.

These results provide useful information for the experimental implementation of the adiabatic quantum simulation of quantum \mathbb{Z}_2 LGT, and its pseudoquantum simulation.

VI. ACKNOWLEDGE

This work was supported by National Science Foundation of China (Grant No. 11574054).

-
- [1] F. J. Wegner, “Duality in generalized ising models and phase transitions without local order parameters,” *J. Math. Phys.* **12**, 2259 (1971).
 - [2] J. B. Kogut, “An introduction to lattice gauge theory and spin systems,” *Rev. Mod. Phys.* **51**, 659 (1979).
 - [3] S. Sachdev, “Topological order, emergent gauge fields, and fermi surface reconstruction,” *Rep. Prog. Phys.* **82**, 014001 (2018).
 - [4] J. Kogut and L. Susskind, “Hamiltonian formulation of Wilson’s lattice gauge theories,” *Phys. Rev. D* **11**, 395–408 (1975).
 - [5] K. G. Wilson, “Confinement of quarks,” *Phys. Rev. D* **10**, 2445–2459 (1974).
 - [6] E. Ercolessi, P. Facchi, G. Magnifico, S. Pascazio, and F. V. Pepe, “Phase transitions in Z_n gauge models: Towards quantum simulations of the schwinger-weyl qed,” *Phys. Rev. D* **98**, 074503 (2018).
 - [7] M. A. Levin and X. G. Wen, “String-net condensation: A physical mechanism for topological phases,” *Phys. Rev. B* **71**, 045110 (2005).
 - [8] X. G. Wen, “An introduction to quantum order, string-net condensation, and emergence of light and fermions,” *Ann. Phys.* **316**, 1 (2005).
 - [9] E. Fradkin, *Field Theories of Condensed Matter Physics*, 2nd ed. (Cambridge University Press, 2013).
 - [10] A. Kitaev, “Fault-tolerant quantum computation by anyons,” *Ann. Phys.* **303**, 2 – 30 (2003).
 - [11] A. Kitaev and C. Laumann, “Topological phases and quantum computation,” arXiv e-prints , arXiv:0904.2771 (2009).

- [12] A. G. Fowler, M. Mariantoni, J. M. Martinis, and A. N. Cleland, “Surface codes: Towards practical large-scale quantum computation,” *Phys. Rev. A* **86** (2012).
- [13] E. Zohar, A. Farace, B. Reznik, and J. I. Cirac, “Digital quantum simulation of $z(2)$ lattice gauge theories with dynamical fermionic matter,” *Phys. Rev. Lett.* **118**, 5 (2017).
- [14] J. Bender, E. Zohar, A. Farace, and J. I. Cirac, “Digital quantum simulation of lattice gauge theories in three spatial dimensions,” *New J. Phys.* **20**, 093001 (2018).
- [15] H. Lamm, S. Lawrence, and Y. Yamauchi (NuQS Collaboration), “General methods for digital quantum simulation of gauge theories,” *Phys. Rev. D* **100**, 034518 (2019).
- [16] C. Schweizer, F. Grusdt, M. Berngruber, L. Barbiero, E. Demler, N. Goldman, I. Bloch, and M. Aidelsburger, “Floquet approach to \mathbb{Z}_2 lattice gauge theories with ultracold atoms in optical lattices,” *Nature Physics* **15**, 1168–1173 (2019).
- [17] X. Cui, J. C. Yang, and Y. Shi, “Circuit-based digital adiabatic quantum simulation and pseudoquantum simulation as new approaches to lattice gauge theory,” *Journal of High Energy Physics* (2020).
- [18] H. F. Trotter, “On the product of semi-groups of operators,” *Proc. Am. Math. Soc.* **10**, 545 (1959).
- [19] S. Lloyd, “Universal quantum simulators,” *Science* **273**, 1073 (1996).
- [20] N. Hatano and M. Suzuki, “Finding exponential product formulas of higher orders,” in *Quantum Annealing and Other Optimization Methods* (Springer Berlin Heidelberg, Berlin, Heidelberg, 2005) p. 37.
- [21] A. M. Childs, Y. Su, M. C. Tran, N. Wiebe, and S. Zhu, “A Theory of Trotter Error,” arXiv e-prints, arXiv:1912.08854 (2019).
- [22] Y. Shi and Y. S. Wu, “Perturbative formulation and nonadiabatic corrections in adiabatic quantum-computing schemes,” *Phys. Rev. A* **69**, 024301 (2004).
- [23] T. Jones, A. Brown, I. Bush, and S. C. Benjamin, “QuEST and High Performance Simulation of Quantum Computers,” *Sci. Rep.* **9**, 10736 (2019).

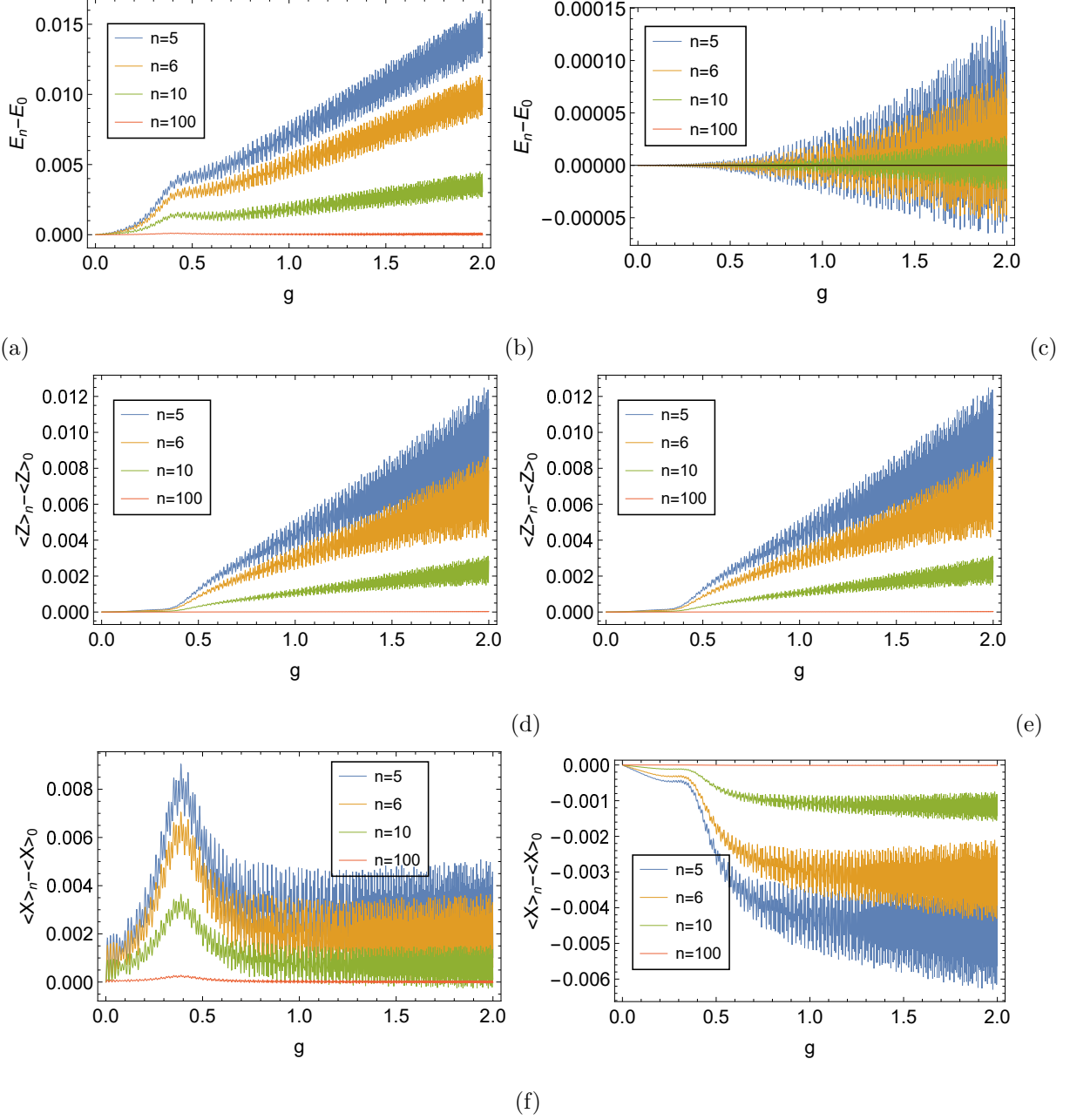


FIG. 4. Numerical results of errors as function of g , in steps of $g_s = 0.001$ with $n = 5, 6, 10, 100$. (a) $E_n - E_0$ in the asymmetric Trotter decomposition. (b) $E_n - E_0$ in the symmetric Trotter decomposition. (c) $\langle Z \rangle_n - \langle Z \rangle_0$ in the asymmetric Trotter decomposition. (d) $\langle Z \rangle_n - \langle Z \rangle_0$ in the symmetric Trotter decomposition. (e) $\langle \mathcal{X} \rangle_n - \langle \mathcal{X} \rangle_0$ in the asymmetric Trotter decomposition. (f) $\langle \mathcal{X} \rangle_n - \langle \mathcal{X} \rangle_0$ in the symmetric Trotter decomposition.

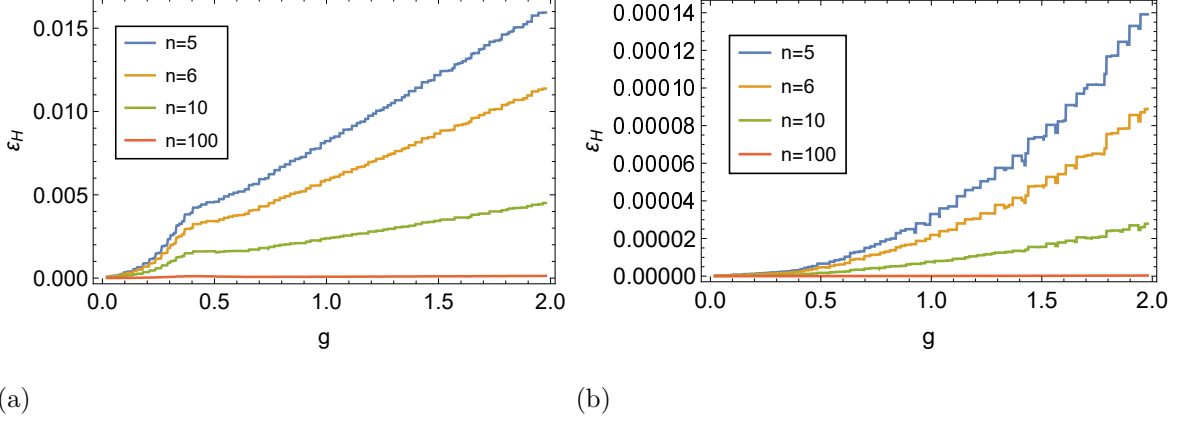


FIG. 5. Error bound ε_H calculated from numerical results of $E_n - E_0$, as a function of g , in step of $g_s = 0.001$ with $n = 5, 6, 10, 100$. (a) Asymmetric Trotter decomposition. (b) Symmetric Trotter decomposition.

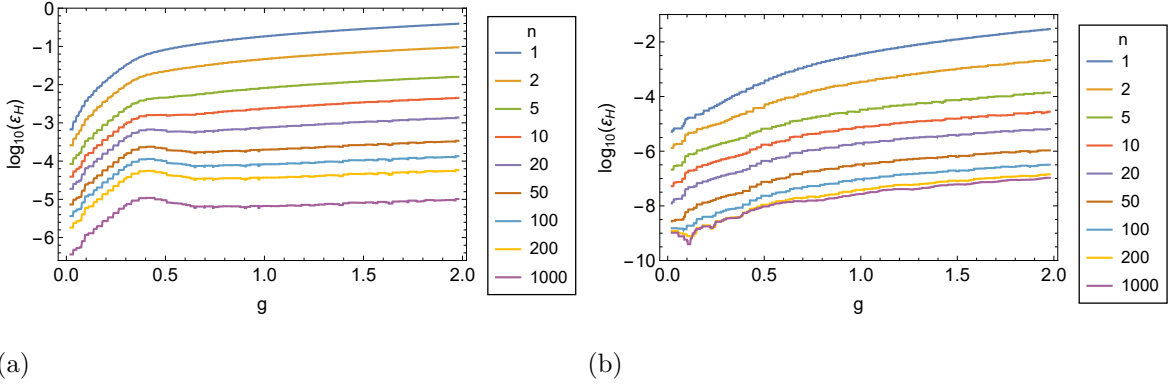


FIG. 6. Numerical results of $\log_{10}(\varepsilon_H)$ as functions of g , in steps of $g_s = 0.001$ with various values of n . (a) Asymmetric Trotter decomposition. (b) Symmetric Trotter decomposition.

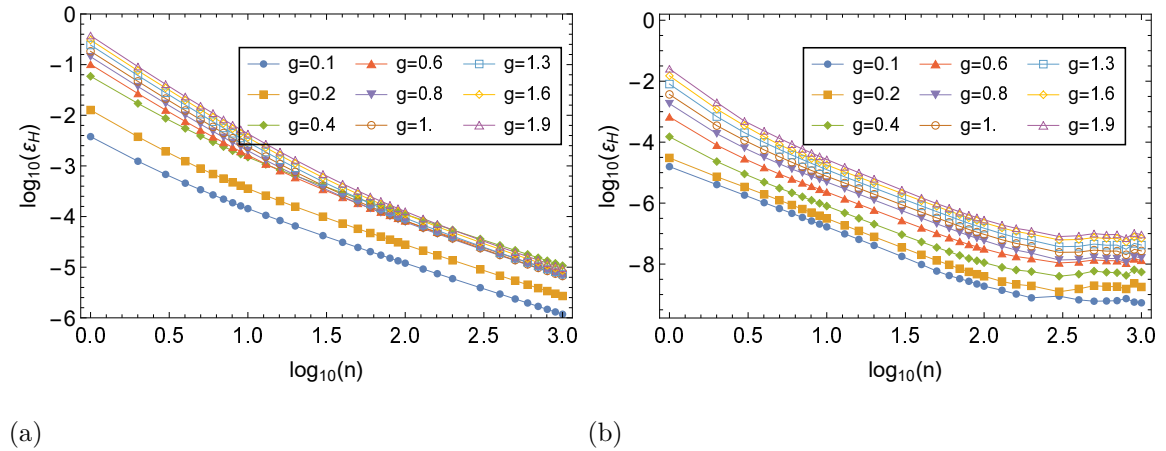


FIG. 7. Numerical results of $\log_{10}(\varepsilon_H)$ as functions of n for various values of g . (a) Asymmetric Trotter decomposition. (b) Symmetric Trotter decomposition.

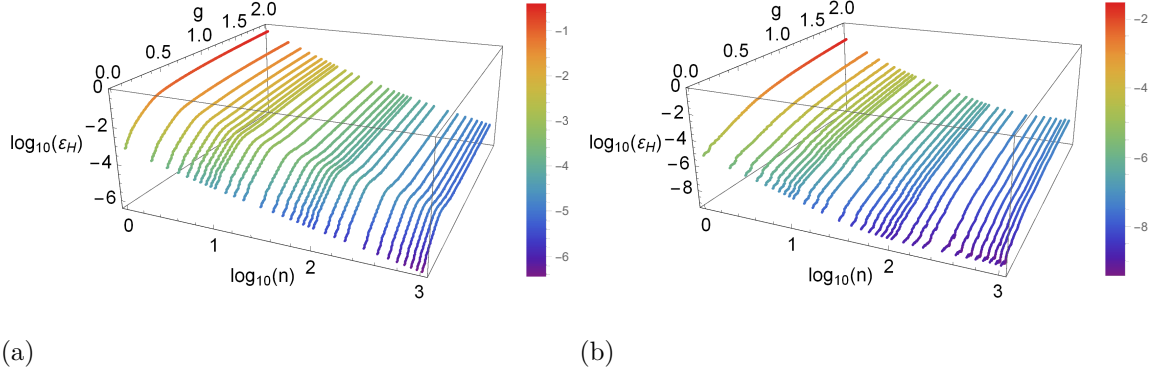


FIG. 8. Numerical results of $\log_{10}(\varepsilon_H)$ as a function of g and $\log_{10}(n)$. g increases from 0 to 2.0 in steps of $g_s = 0.001$ and $t_s = 0.1$, while $\log_{10}(n)$ increases from 0 to 3. (a) Asymmetric Trotter decomposition. (b) Symmetric Trotter decomposition.

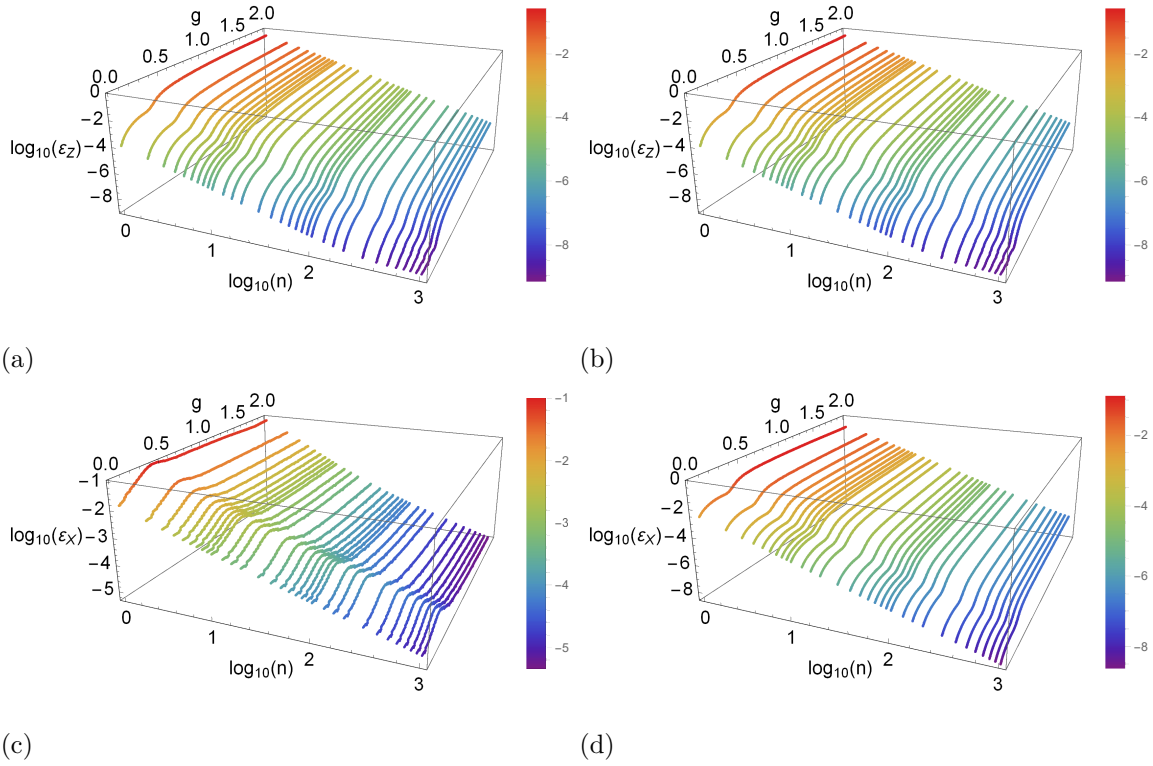


FIG. 9. Numerical results of $\log_{10}(\varepsilon_Z)$ and $\log_{10}(\varepsilon_X)$ as functions of g , which increases from 0 to 2.0 in step of $g_s = 0.001$ and $t_s = 0.1$, and $\log_{10}(n)$, which increases from 0 to 3. (a) $\log_{10}(\varepsilon_Z)$ in the asymmetric Trotter decomposition. (b) $\log_{10}(\varepsilon_Z)$ in the symmetric Trotter decomposition. (c) $\log_{10}(\varepsilon_X)$ in the asymmetric Trotter decomposition. (d) $\log_{10}(\varepsilon_X)$ in the symmetric Trotter decomposition.

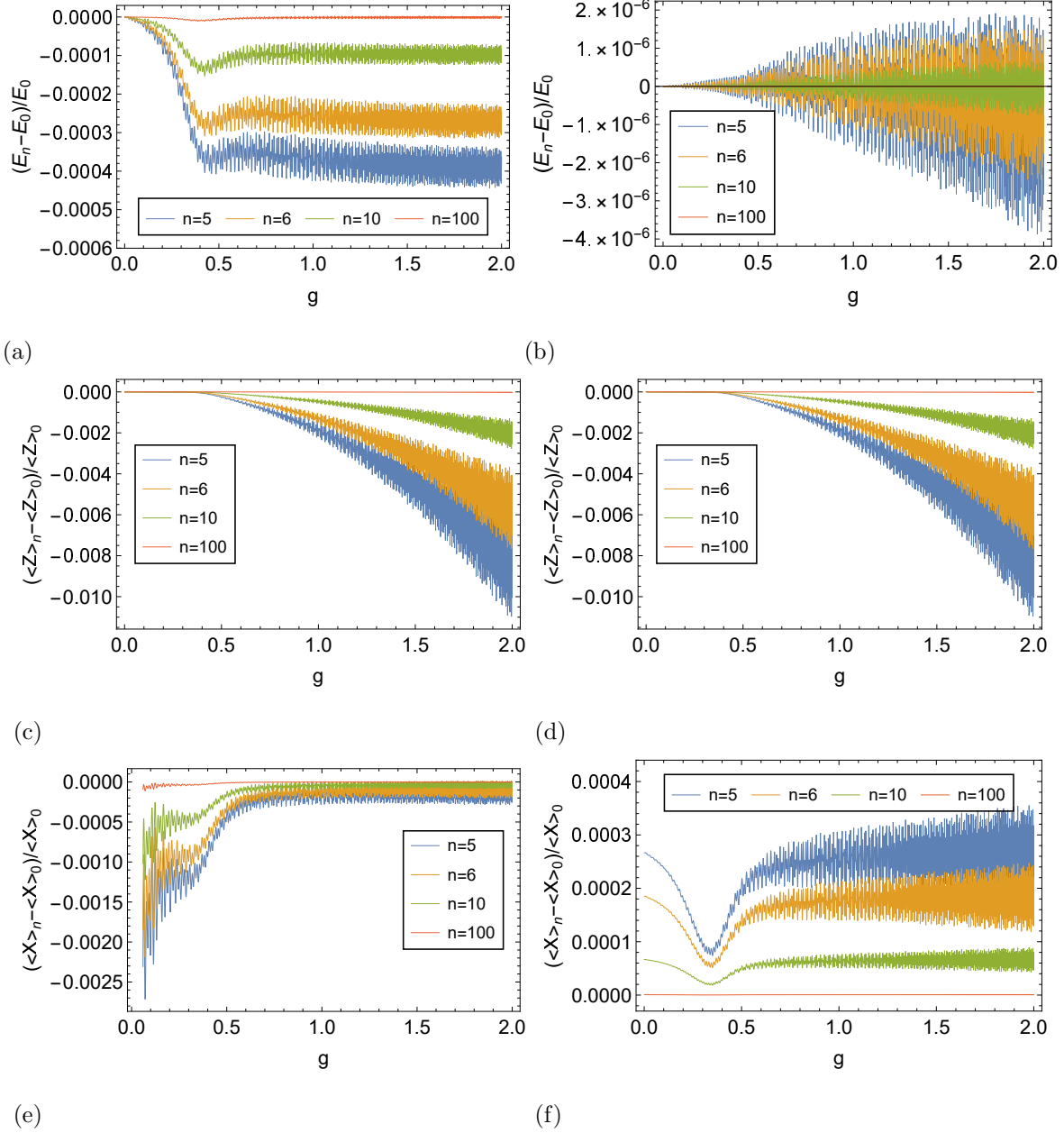
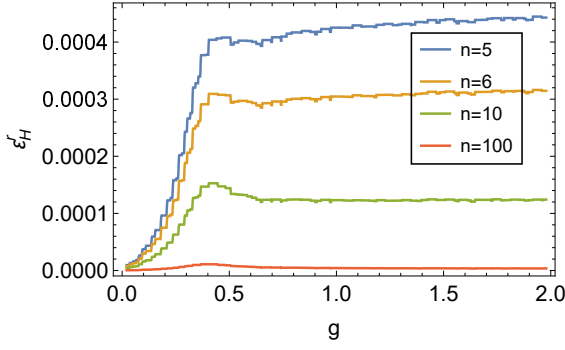
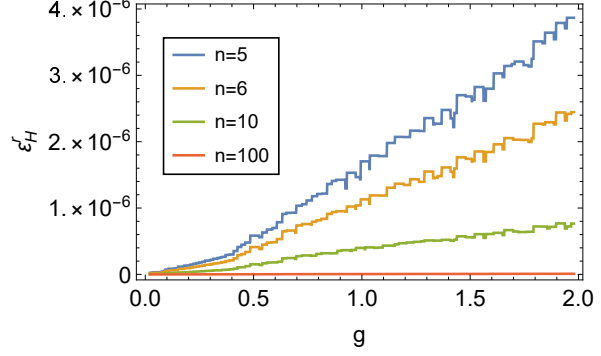


FIG. 10. Numerical results of relative errors as function of g , in steps of $g_s = 0.001$ with $n = 5, 6, 10, 100$. (a) $(E_n - E_0)/E_0$ in the asymmetric Trotter decomposition. (b) $(E_n - E_0)/E_0$ in the symmetric Trotter decomposition. (c) $(\langle Z \rangle_n - \langle Z \rangle_0)/\langle Z \rangle_0$ in the asymmetric Trotter decomposition. (d) $(\langle Z \rangle_n - \langle Z \rangle_0)/\langle Z \rangle_0$ in the symmetric Trotter decomposition. (e) $(\langle X \rangle_n - \langle X \rangle_0)/\langle X \rangle_0$ in the asymmetric Trotter decomposition. (f) $(\langle X \rangle_n - \langle X \rangle_0)/\langle X \rangle_0$ in the symmetric Trotter decomposition.

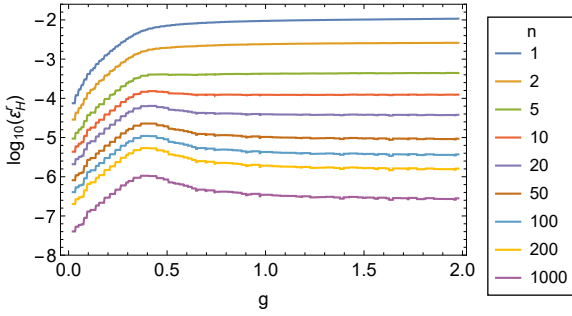


(a)

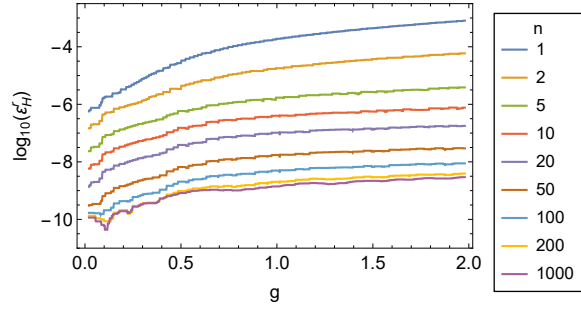


(b)

FIG. 11. Relative error bound ε_H^r calculated from numerical results of $(E_n - E_0)/E_0$, as a function of g , in step of $g_s = 0.001$ with $n = 5, 6, 10, 100$. (a) Asymmetric Trotter decomposition. (b) Symmetric Trotter decomposition.

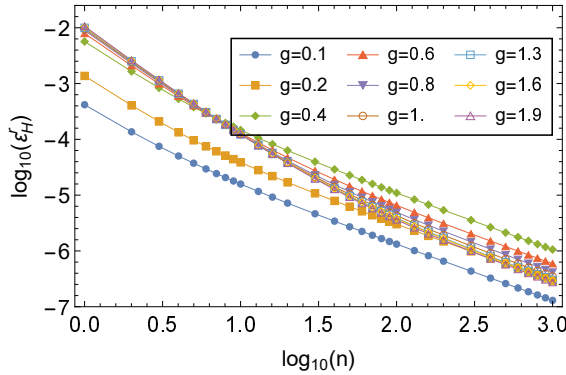


(a)

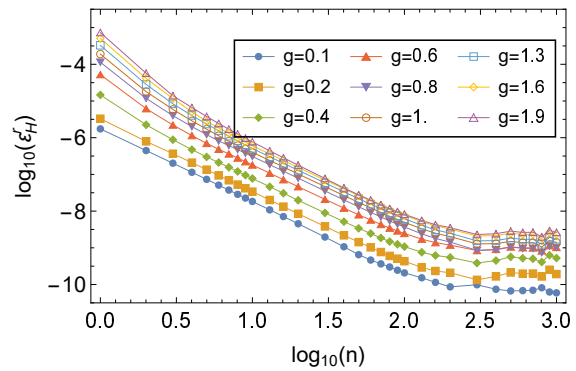


(b)

FIG. 12. Numerical results of $\log_{10}(\varepsilon_H^r)$ as functions of g , in steps of $g_s = 0.001$ with various values of n . (a) Asymmetric Trotter decomposition. (b) Symmetric Trotter decomposition.



(a)



(b)

FIG. 13. Numerical results of $\log_{10}(\varepsilon_H^r)$ as functions of n for various values of g . (a) Asymmetric Trotter decomposition. (b) Symmetric Trotter decomposition.

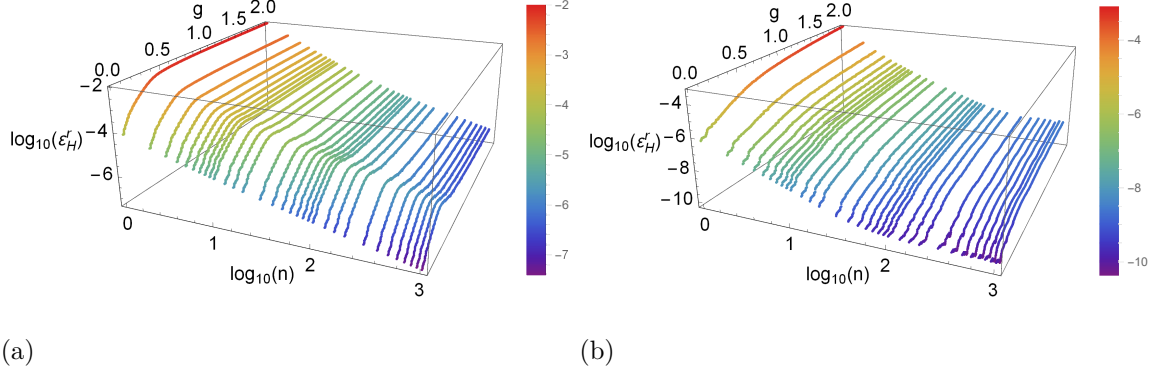


FIG. 14. Numerical results of $\log_{10}(\varepsilon_H^r)$ as a function of g and $\log_{10}(n)$. g increases from 0 to 2.0 in steps of $g_s = 0.001$ and $t_s = 0.1$, while $\log_{10}(n)$ increases from 0 to 3. (a) Asymmetric Trotter decomposition. (b) Symmetric Trotter decomposition.

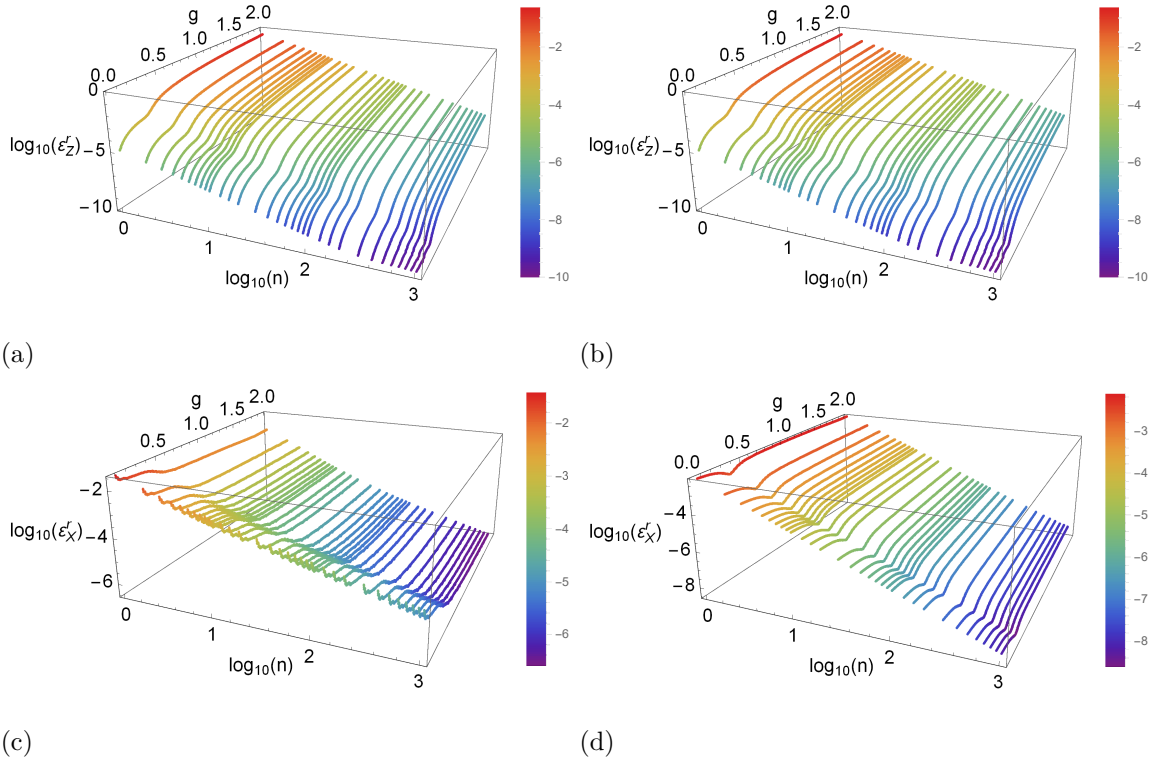


FIG. 15. Numerical results of $\log_{10}(\varepsilon_Z^r)$ and $\log_{10}(\varepsilon_X^r)$ as functions of g , which increases from 0 to 2.0 in step of $g_s = 0.001$ and $t_s = 0.1$, and $\log_{10}(n)$, which increases from 0 to 3. (a) $\log_{10}(\varepsilon_Z^r)$ in the asymmetric Trotter decomposition. (b) $\log_{10}(\varepsilon_Z^r)$ in the symmetric Trotter decomposition. (c) $\log_{10}(\varepsilon_X^r)$ in the asymmetric Trotter decomposition. (d) $\log_{10}(\varepsilon_X^r)$ in the symmetric Trotter decomposition.